A general locomotion control framework for serially connected multi-legged robots

Journal Title
XX(X):1–15

DOI: 10.1177/ToBeAssigned
www.sagepub.com/
SAGE

Baxi Chong[1*], Yasemin O. Aydin[1*], Jennifer M. Rieser[2], Guillaume Sartoretti[3], Tianyu Wang[1], Julian Whitman[4], Abdul Kaba[5], Enes Aydin[1], Ciera McFarland[6], Howie Choset [4], Daniel I. Goldman[1]

Abstract

Serially connected robots are promising candidates for performing tasks in confined spaces such as search-and-rescue in large-scale disasters. Such robots are typically limbless, and we hypothesize that the addition of limbs could improve mobility. However, a challenge in designing and controlling such devices lies in the coordination of high-dimensional redundant modules in a way that improves mobility. Here we develop a general framework to control serially connected multi-legged robots. Specifically, we combine two approaches to build a general shape control scheme which can provide baseline patterns of self-deformation ("gaits") for effective locomotion in diverse robot morphologies. First, we take inspiration from a dimensionality reduction and a biological gait classification scheme to generate cyclic patterns of body deformation and foot lifting/lowering, which facilitate generation of arbitrary substrate contact patterns. Second, we use geometric mechanics methods to facilitates identification of optimal phasing of these undulations to maximize speed and/or stability. Our scheme allows the development of effective gaits in multi-legged robots locomoting on flat frictional terrain with diverse number of limbs (4, 6, 16, and even 0 limbs) and body actuation capabilities (including sidewinding gaits on limbless devices). By properly coordinating the body undulation and the leg placement, our framework combines the advantages of both limbless robots (modularity) and legged robots (mobility). We expect that our framework can provide general control schemes for the rapid deployment of general multi-legged robots, paving the ways toward machines that can traverse complex environments under real-life conditions.

Keywords

Class file, LaTeX 2$_\varepsilon$, *SAGE Publications*

Introduction

Robots with certain shapes (e.g., rigid boxes or multi-link systems) and limb numbers (monopod hoppers to 6 and 12 legged crawlers) have advantages in different specific applications, such as quadrupeds for agility Tan et al. (2018), hexapods and myriapods for stability Aoi et al. (2016); Saranli et al. (2001), and limbless robots for confined spaces McKenna et al. (2008). The ability to design and construct robots with increasing complexity and numbers of DoF presents interesting challenges in motion coordination, which if not addressed, may render complex robots unusable. Furthermore, the diversity of shape and form makes it challenging to transfer control insights gained on one platform onto another. Taken together, we arrive at a situation where there is limited intuition and physical understanding of how to coordinate these DoF to generate effective motion for complex robots.

To address the growing need to control robots with different shapes, modular robot control strikes a balance between encompassing a broad variety of shapes while still being able to precisely control them Wright et al. (2007); Tesch et al. (2009). Modular robot control has been successfully used in serially connected limbless robots where a single control principle can be applied in robots with different sizes Sartoretti et al. (2019). In contrast, the study of modular control in legged robots has been limited.

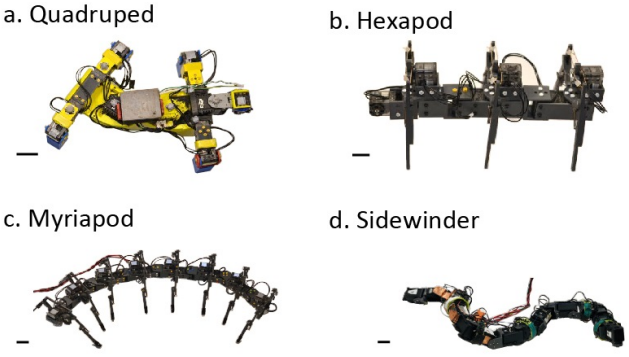

Figure 1. Legged and limbless robotic models studied in the paper. a. Quadrupedal robot Ozkan Aydin et al. (2017); Chong et al. (2021) b. Hexapod robot c. Myriapod robot with eight pairs of legs Ozkan-Aydin et al. (2020*a*) d. Sidewinder robot Astley, Rieser, Kaba, Paez, Tomkinson, Mendelson and Goldman (2020*a*). All scale bars are 5 cm. See Fig. S4 for the axis of joint angles.

[1]Georgia Institute of Technology [2] Emory University [3] National University of Singapore [4] Carnegie Mellon University [5] Morehouse College [6] Pennsylvania State University [*] Equal contribution

Corresponding author:
Corresponding author: Daniel I. Goldman
Email: daniel.goldman@physics.gatech.edu

The challenge in serially connected multi-legged robots lies not only in designing the stepping patterns of legs, but also in the coordination between the body and legs. For example, in robots that mix limbs and body undulation, if stepping patterns and body undulations are not properly coordinated, limbs can interfere with each other, resulting in reduced locomotion performance, instability, or even failure Mazouchova et al. (2013); Byl (2008).

We would like to develop control schemes to generate appropriate periodic "self-deformation patterns" (defined as relative movement of body and limb elements) for the general class of serially connected robots. Over the past decades, many techniques (e.g., gait generation Wettergreen and Thorpe (1992); Sun and Metaxas (2001), central pattern generators Ijspeert et al. (2007); Crespi et al. (2008), nearest limb synchronization Dutta et al. (2019) and unsupervised machine learning Tan et al. (2018); Hwangbo et al. (2019)) have been developed to control legged and limbless robots Saranli et al. (2001); Park et al. (2017); Hatton et al. (2013); Marvi et al. (2014); Ijspeert et al. (2007). In this paper, we take inspiration from living systems: organisms with diverse numbers of appendages and body plans exhibit effective locomotion on almost all terrestrial environments Farley and Ko (1997); Popovic et al. (2005); Marvi et al. (2014), and do so by making/breaking the ground contact with limbs (e.g., salamanders) and bodies (e.g., sidewinders), in conjunction with waves of undulation.

Some of the complexity of legged locomotion was tamed in the last century via a classification scheme called "Hildebrand diagrams". Hildebrand Hildebrand (1965) developed schemes to study symmetrical gaits * observed in quadrupeds. These gaits have two key variables: *duty factor*, the fraction of a period that each leg is on the ground over a full gait cycle, and *lateral phase lag*, the fraction of a period that the hind leg leads the foreleg on the same side. It has been reported that both key variables are modulated in response to speed changes in biological Hildebrand (1980) and robotics systems Owaki et al. (2013). Using these gait principles as a reference, a multitude of algorithms were developed and implemented on quadrupedal robots to traverse various environments McGhee and Frank (1968); Bai et al. (1999); Owaki et al. (2013); Kalakrishnan et al. (2010); Bellicoso et al. (2018); Hoyt and Taylor (1981). But thus far, such gait principles have not been applied to robots with greater numbers of appendages.

In biological locomotors and increasingly in robots, appendages that make direct contact with substrates are not the sole contributor to locomotion. It has been shown that undulatory body motions play an important role in generating propulsive forces in many systems Kafkafi and Golani (1998); Farley and Ko (1997); Frolich and Biewener (1992); Manton (1952). For undulatory locomotors, the geometric mechanics community Kelly and Murray (1995); Ostrowski and Burdick (1998); Shapere and Wilczek (1989); Shammas et al. (2007); Hatton and Choset (2015); Astley et al. (2015); Chong et al. (2021); Gong et al. (2018) has developed a gait design framework to prescribe self-deformations of limbless systems immersed on continuous media such as 3-link robots, lizards, and snakes Rieser et al. (2019); Hatton and Choset (2015); Hatton et al. (2013); and in discontinuous settings including sidewinders Astley, Mendelson, Dai, Gong, Chong, Rieser, Schiebel, Sharpe, Hatton, Choset et al. (2020); Astley, Rieser, Kaba, Paez, Tomkinson, Mendelson and Goldman (2020*b*). While mathematically elegant, geometric mechanics has limitations. In particular, it is not directly applicable to systems with a large number of DoF. Therefore, some forms of dimensionality reduction are required to simplify the locomotion kinematics. For example, by prescribing the body undulation in multi-segment robot as a traveling wave, geometric mechanics offers the tool to analyze, predict, and optimize the body undulation patterns in coordination with the contact patterns for both biological Rieser et al. (2019); Astley, Mendelson, Dai, Gong, Chong, Rieser, Schiebel, Sharpe, Hatton, Choset et al. (2020) and robotics systems Astley et al. (2015).

In this paper, we integrate dimensionality reduction techniques with tools from geometric mechanics to develop locomotion control schemes for general serially connected robots. We first develop an extended Hildebrand gait classification scheme to prescribe a wide range of contact patterns (the sequenced of making/breaking contacts with environments) by the Hildebrand parameters (duty factor and lateral phase lag). Using the extended Hildebrand scheme to reduce dimensionality and by prescribing body undulation as a traveling wave, we apply geometric mechanics to coordinate the lateral body undulation and the body contact patterns. We evaluate the gait performance based on speed and static stability, and investigate the relationship between these metrics of gait performance and the Hildebrand parameters. We demonstrate our motion control framework on robots with 4 (quadrupeds), 6 (hexapod), 16 (myriapod-like), and even 0 (sidewinders) limbs (Fig. 1), revealing empirical rules to balance the trade-off between speed and stability, and the potential benefit of body undulation in multi-legged robot locomotion. In this way, our framework offers the potential to modulate gaits for different tasks by switching between fast gaits and stable gaits. Moreover, by properly coordinating lateral body undulation and leg movement, our framework leverages advantages from both legged and limbless robots. Specifically, by introducing waves in both limb contact and lateral body undulation, our framework facilitates centralized modular control of serially connected multi-legged robots. On the other hand, by properly lifting and landing body segments, our framework can greatly improve the mobility of limbless robots. In this way, we posit that our scheme can then serve as the basis towards the coordination, trade-off of stability and speed in serially connected multi-legged robots.

Hildebrand Gait Prescription

Prescription of Quadrupedal Contact Pattern

Hildebrand Hildebrand (1965) introduced a scheme to describe symmetric quadrupedal gaits. In the Hildebrand gait formulation, symmetric quadrupedal gaits are categorized by two parameters: the duty factor (D), which represents the fraction over a gait period that each leg is on the ground,

*In symmetric gaits, the contralateral (the left and right pair of legs) legs are 180° out of phase.

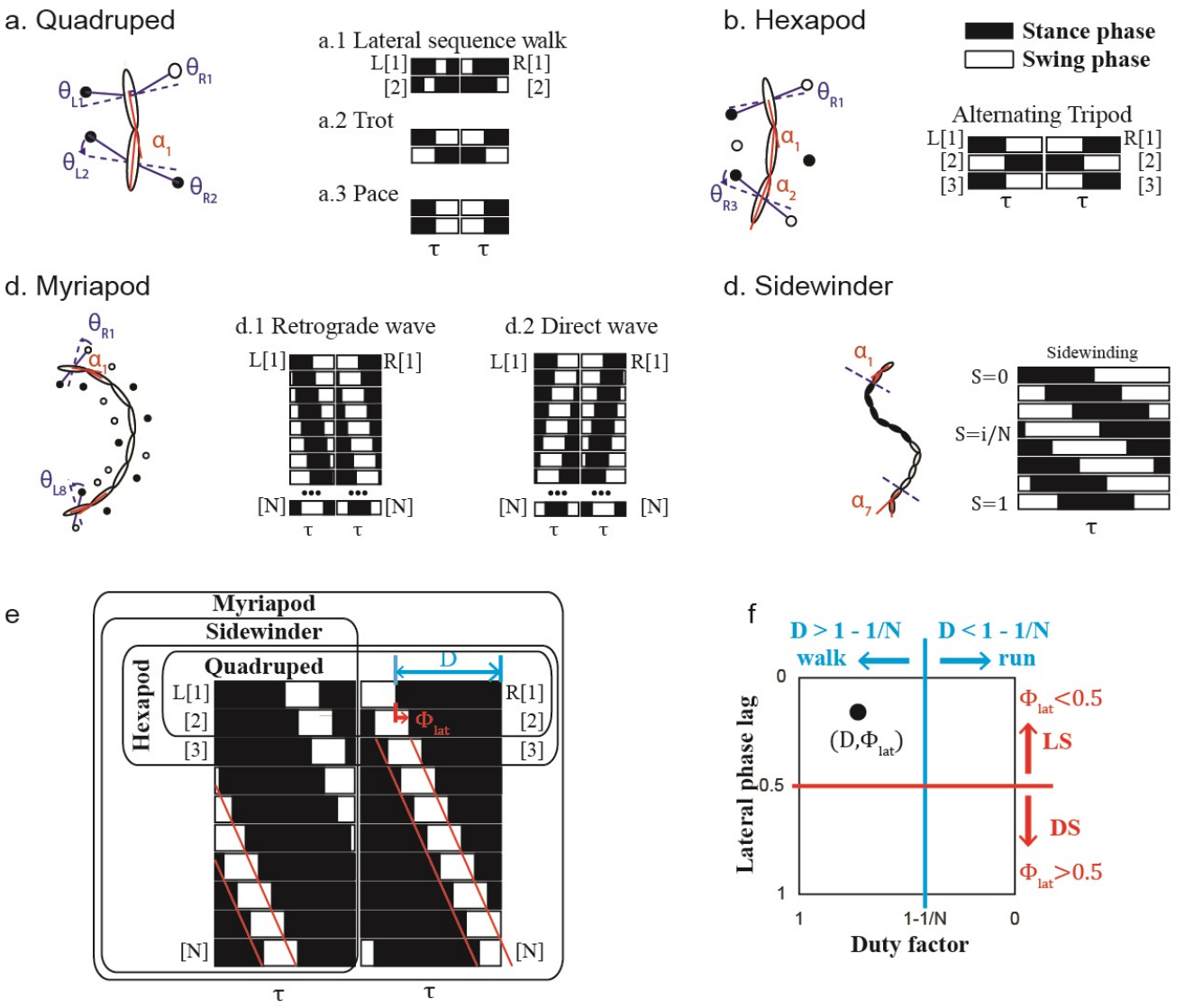

Figure 2. General description of multi-legged systems and sidewinders. The body contact patterns of some well-known gaits: (a.1) lateral sequence walking, (a.2) trotting, and (a.3) pacing of quadrupeds; (b) alternating tripod of hexapods, (c) sidewinding of sidewinder limbless robots, (d.1) retrograde-wave of and (d.2) direct-wave of myriapods. Cartoons show the shape variables (the leg joint angles, θ_N, and body joint angles, $\alpha_{(N-1)}$ where N is the number of leg pairs for legged systems and the implicit legged system (sidewinder). Filled blocks represent stance phase, open blocks represent swing phase. (e) The general contact pattern table. The blue arrow represents the duty factor D. The red arrow represents the lateral phase lag, Φ_{lat}. τ denote gait phase (f) Hildebrand plots with two parameters D and Φ_{lat} to characterize the motions in the vertical plane. We labeled the region of walk, run, lateral sequence and diagonal sequence.

and the lateral phase lag (Φ_{lat}), which represents the fraction over a gait period that the hind leg leads the foreleg on the same side. There are three major assumptions in the Hildebrand symmetric gait family: (1) the duty factor of each leg is the same, (2) the pair of contralateral legs are 180° out of phase, and (3) the lateral phase lag is the same for left and right legs.

We use a binary variable c to represent the contact state of a leg, where $c = 1$ represents the stance phase and $c = 0$ represents the swing phase. The contact pattern of symmetric quadrupedal gaits can be written as

$$
\begin{aligned}
c_{FL}(\phi_c) &= \begin{cases} 1, & \text{if } \mathrm{mod}(\phi_c, 2\pi) < 2\pi D \\ 0, & \text{otherwise} \end{cases} \\
c_{FR}(\phi_c) &= c_{FL}(\phi_c + \pi) \\
c_{HL}(\phi_c) &= c_{FL}(\phi_c - 2\pi\Phi_{lat}) \\
c_{HR}(\phi_c) &= c_{FL}(\phi_c - 2\pi\Phi_{lat} + \pi)
\end{aligned} \tag{1}
$$

where Φ_{lat} denotes the lateral phase lag and D denotes the duty factor, $c_{FL}(\phi_c)$, $c_{FR}(\phi_c)$, $c_{HL}(\phi_c)$, and $c_{HR}(\phi_c)$ denote the contact state of the fore-right (FR), fore-left (FL), hind-left (HL), and hind-right (HR) limbs at the gait phase ϕ_c, respectively. Many commonly seen quadrupedal gaits can be described using the Hildebrand formula. For example, the lateral sequence walking gait (Fig. 2), can be described by $D = 0.75$, $\Phi_{lat} = 0.25$, where each leg is lifted for a quarter

of a cycle and only one leg is lifted at any given instant; the leg lifting sequence follows FR, HR, FL, and HR. The quadrupedal trot gait (Fig. 2) can be described by $D = 0.5$, $\Phi_{lat} = 0.5$, where the FR and HL are coupled in phase (same as the FL and HR pair). Another quadrupedal gait, the pace gait (Fig. 2), can be described by $D = 0.5$, $\Phi_{lat} = 0$, where the FR and HR are coupled in phase, as are the FL and HL pair. Note that there are also asymmetric quadrupedal gaits which cannot be prescribed by Hildebrand methods, such as bounding and galloping.

Prescription of General Contact Pattern for Arbitrary Robots

The first two assumptions of Hildebrand symmetric gait family holds for the general discrete contact systems; and we can generalize the definition of the lateral phase lag to a broader range of locomotors by defining lateral phase lag as the phase lag between two consecutive legs (instead of the fore and hind legs) on the same side. Then, the contact function of a multi-legged system can be written as:

$$
\begin{aligned}
c_l(\phi_c, 1) &= \begin{cases} 1, & \text{if mod}(\phi_c, 2\pi) < 2\pi D \\ 0, & \text{otherwise} \end{cases} \\
c_l(\phi_c, i) &= c_l(\phi_c - 2\pi(i-1)\Phi_{lat}, 1) \\
c_r(\phi_c, i) &= c_l(\phi_c + \pi, i),
\end{aligned} \tag{2}
$$

where $c_l(\phi_c, i)$ (and $c_r(\phi_c, i)$) denotes the contact state of i-th leg on the left (and the right) at gait phase ϕ_c, $i \in \{1, ...N\}$ for $2N$-legged systems.

Many commonly developed multi-legged gaits can also be described by this extended contact formulation. For example, most hexapod robots and animals use the alternating tripod gait (Fig. 2), which couples FL, MR (middle-right), and HL in phase, and couples the FR, ML, and HR similarly. The alternating tripod gait for a hexapod ($N = 3$) can be described by $D = 0.5$ and $\Phi_{lat} = 0.5$.

Myriapod gaits can be classified into direct waves and retrograde waves of limb contact Kuroda et al. (2014) (Fig. 2). Typically, for gaits with $\Phi_{lat} < 0.5$, the phase of the hind leg is ahead of the phase of its immediate fore leg. In other words, the legs move in a wave pattern propagating from tail to head, which we call a diagonal sequence gait (corresponding to direct waves in myriapods). On the other hand, when $\Phi_{lat} > 0.5$, the phase of the hind leg is behind the phase of its immediate fore leg. Therefore, the leg wave propagates from head to tail, which we call a lateral sequence gait (corresponding to retrograde waves in myriapods). Interestingly, animals with fewer legs have been seen to more commonly use lateral sequence gaits Hildebrand (1965, 1967, 1980), and animals with more legs are observed to use both diagonal sequence and lateral sequence gaits Manton (1952); Anderson et al. (1995). As we will discuss later, we hypothesize that this difference in gait choice is a result of the balance between speed and stability.

Our proposed gait formulation can also include systems without legs, e.g., sidewinding limbless robots. The complex mode of limbless locomotion, sidewinding, can be prescribed as the superposition of two waves: lateral and vertical body waves Astley et al. (2015). Similar to legged systems, sidewinders can regulate their contacts by modulating the vertical traveling wave Astley et al. (2015). The typical contact pattern of sidewinder is shown in Fig. 2. Note that the contact pattern during sidewinding locomotion is the same as one side (either left or right) of the contact pattern of a multi-legged system. As such, we prescribe the contact state of the i-th link of the sidewinding system as $c(\phi_c, i) = c_l(\phi_c, i)$, where $c_l(\phi_c, i)$ is defined in Eq. 2

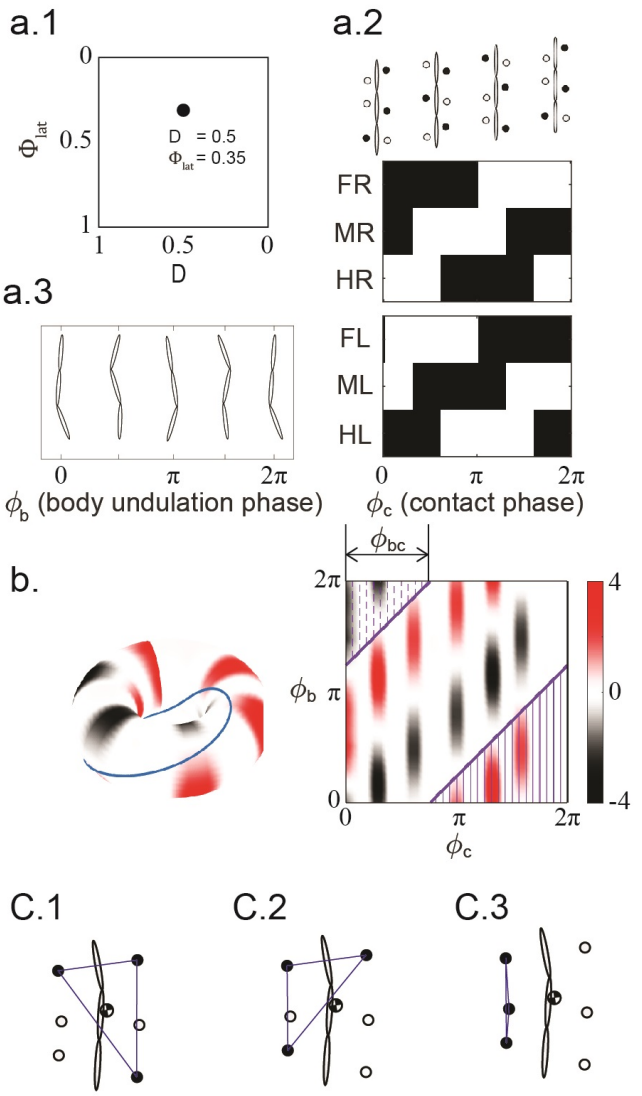

Figure 3. An example of gait design for a hexapod using Hildebrand gait principles. From the parameter space (a.1), we select the duty factor D and lateral phase lag Φ_{lat}. We prescribe the contact by its phase ϕ_c (a.2), and the lateral body undulation by its phase ϕ_b (a.3). (b) The height functions to design gait. The gait path (the purple curve) is designed to maximize the volume enclosed in the lower right corner (in solid shadow) minus the volume enclosed in the upper left corner (in dashed shadow). We illustrated the typical configurations that the robot is statically stable (c.1), statically unstable (c.2) and unstable (c.3)

Prescription of Leg Shoulder Movement

Legs generate self-propulsion by protracting during the stance phase, where they make contact with environments and retracting during the swing phase, where they break contact with environments. That is, the leg moves from the anterior to the posterior end during the stance phase and

moves from the posterior to anterior end during the swing phase. With this in mind, we use a piece-wise sinusoidal function to prescribe the leg shoulder angle (θ, Fig. 2) for a given contact phase (ϕ_c),

$$\theta_l(\phi_c, 1) = \begin{cases} A_\theta \cos\left(\frac{\phi_c}{2D}\right), & \text{if } \mathrm{mod}(\phi_c, 2\pi) < 2\pi D \\ -A_\theta \cos\left(\frac{\phi_c - 2\pi D}{2(1-D)}\right), & \text{otherwise,} \end{cases}$$
$$\theta_l(\phi_c, i) = \theta_l(\phi_c - 2\pi(i-j)\Phi_{lat}, j)$$
$$\theta_r(\phi_c, i) = \theta_r(\phi_c + \pi, i) \quad (3)$$

where A_θ is the shoulder angle amplitude, $\theta_l(\phi_c, i)$ and $\theta_r(\phi_c, i)$ denote the leg shoulder angle of i-th left and right leg at contact phase ϕ_c, respectively. Note that the shoulder angle is maximum ($\theta = A_\theta$) at the transition from swing to stance phase, and is minimum ($\theta = -A_\theta$) at the transition from stance to swing phase. Fig. 3 shows an example of a hexapod gait under this equation.

Numerical Prediction on Speed and Stability

We numerically calculated the speed of various gaits Hatton and Choset (2015) over a range duty factors and lateral phase lags for a quadruped, hexapod, myriapod, and sidewinder systems (Fig. 3 and Fig. 4 for a graphical depiction of the process, and the Materials and Methods section for details). To explicitly show the effect of limb-substrate contact on speed, we fixed the swing angle A_θ when comparing the displacements of different gait parameters. Note that in this section, there is no body undulation in all gaits.

The numerical prediction of body speed, measured in units of body length per cycle (BLC), is plotted in Fig. 5 (middle colomn). We observe that modulating the lateral phase lag does not significantly affect speed. This observation becomes more apparent for systems with more legs. In the myriapod system, speed is almost independent of the lateral phase lag and is uniquely determined by the duty factor.

In addition to measuring body speed, we require other metrics to quantify gait stability. For instance, the contact pattern of quasi-static gaits (e.g., quadrupedal walking gaits) need significantly less low-level control efforts to be stably realized on robots than the contact pattern of dynamically stable gaits (e.g., bouncing gaits) McGhee and Frank (1968). In this paper, we separate robots' configurations into three groups (1) statically stable, (2) statically unstable, and (3) unstable. In the statically stable configurations, the center of mass is bounded within the supporting polygon (Fig. 3c.1). In the statically unstable configurations, also known as unstable diagonal-couplet gaits Hildebrand (1967), the center of mass is outside the supporting polygon but there is at least one leg in stance phase on the left and the right side (Fig. 3c.2). Despite not being statically stable, the statically unstable configurations can be made dynamically stable when the speed increases Hildebrand (1980) or when combined with a low-level controller Kalakrishnan et al. (2010); Park et al. (2017); Bellicoso et al. (2018). In other words, the loss of static stability could be compensated by the acquired dynamic stability. In the unstable configurations, also known as unstable lateral-couplet gaits Hildebrand (1967), either the left or the right side of the legs are all in swing phase (Fig. 3c.3), which significantly raises the difficulties to stably implemented (in the sidewinding case, the unstable configuration are defined as no contact condition, Fig. S4). We define the static stability as the fraction of the gait cycle spent in statically stable configurations. Note that this measure only applies to the gaits with statically stable and statically unstable configurations; the appearance of unstable configurations will contradict our assumptions. Therefore, we define the measure of static stability to be 0 if there exists unstable configurations in the gait.

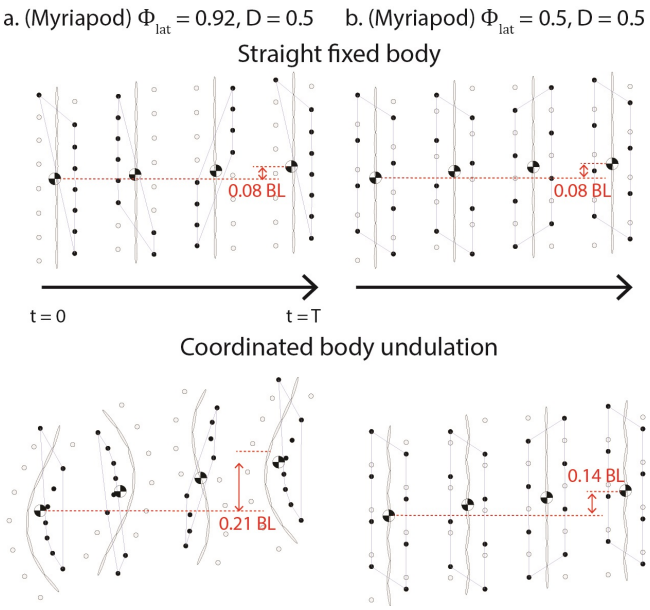

Figure 4. Snapshots of the numerical simulation showing examples of two prescribed myriapod gaits. (a) statically unstable, $\Phi_{lat} = 0.92$, $D = 0.5$ and (b) statically stable $\Phi_{lat} = 0.5$, $D = 0.5$. We compared the gait with straight fixed body (top) and gaits with coordinated body undulation (bottom). The displacement (unit: body length per cycle) were labeled in red arrow. The black (on ground) and white (in air) circles show the state of the legs.

Static stability for the quadruped, hexapod, and myriapod systems are depicted in Fig. 5. As one might expect, when comparing the same gait parameters among different systems, the static stability increases with the number of legs. Similarly, an increase in duty factor results in an increase in static stability. Moreover, we observe that the diagonal sequence ($\Phi_{lat} > 0.5$) is in general less stable than the lateral sequence ($\Phi_{lat} < 0.5$). For most gaits, diagonal sequence gaits are only stable for systems with a greater number of legs, such as myriapods. The static stability is also strongly correlated with the lateral phase lag. Specifically, gaits are more statically stable as $|\Phi_{lat} - 0.5| \to 0$ and they become "closer" to an alternating tripod gait.

Surprisingly, modulating the lateral phase lag only affects the static stability, while body speed is not correlated with the lateral phase lag. On the other hand, animals including myriapods Manton (1952) and lizards Farley and Ko (1997) have been observed to modulate the lateral phase lag as speed increases. In other words, in biological systems, the loss of static stability is compensated by a gain in speed. In this way, we hypothesize that lateral phase lag modulation does not directly affect the speed. Instead, there should be a mechanism such that the lateral phase lag modulation can affect the speed through whole-body coordination.

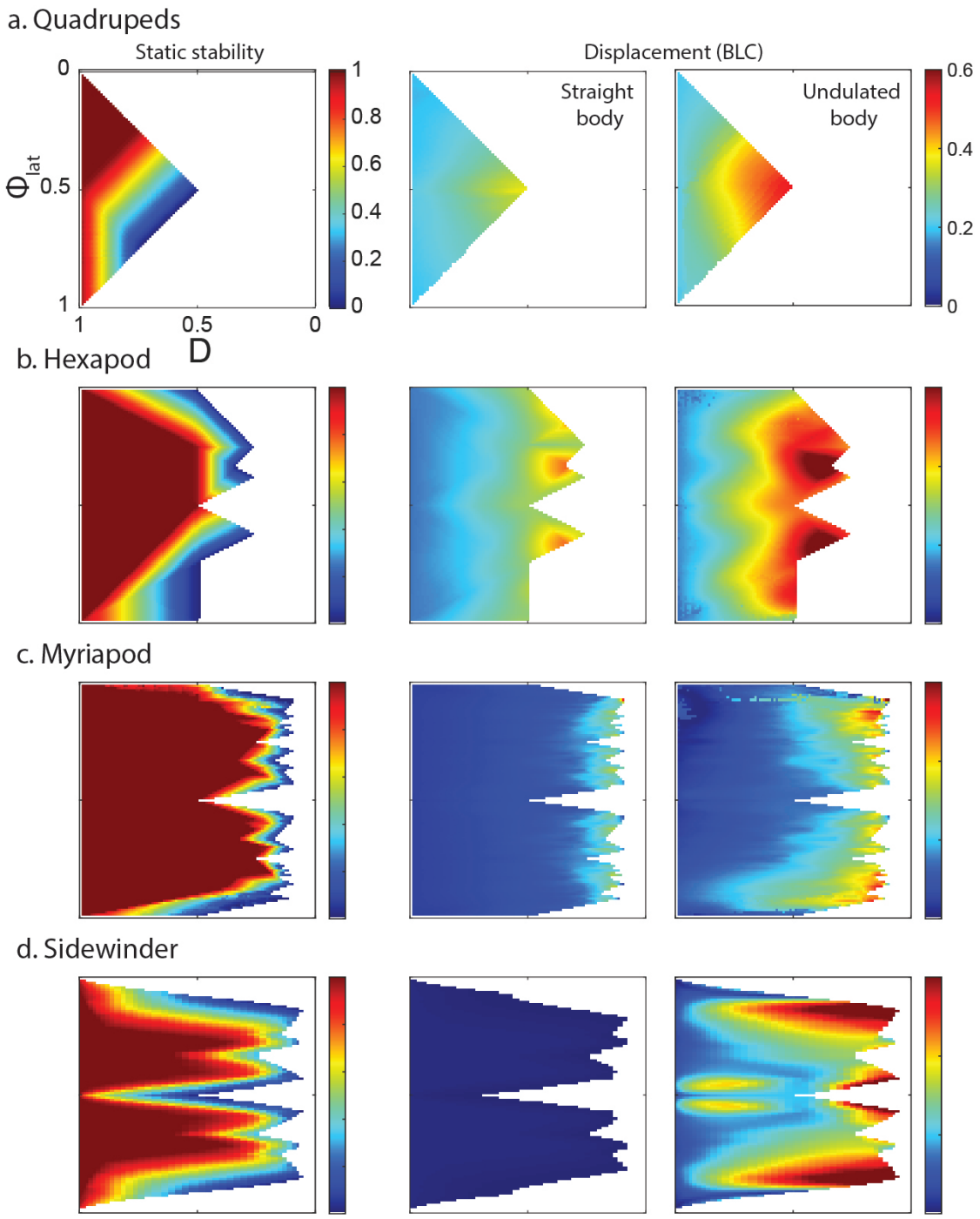

Figure 5. Trade-off between speed and static stability in quadruped, hexapod, myriapod, and sidewinding systems. Theoretically predicted static stability (left panel), displacement (BLC) with fixed straight back (middle panel), and displacement (BLC) with coordinated lateral body undulation (right panel) over the Hildebrand plot (D vs. Φ_{lat}) for quadrupeds (a), hexapod (b), myriapod (c) and sidewinder (d). White space in all panels represents the space where there exists unstable configurations (Fig. 3c.3) and therefore static stability is defined to be zero. Note that static stability of quadruped, hexapod and myriapod is numerically calculated for system with fixed straight back. The static stability of sidewinder is numerically calculated for system with coordinated lateral body undulation. Note that we only consider gaits where there the unstable configurations (Fig. 3c.3) do not occur.

Experimental Results on Speed and Stability

Using robophysical models, we tested the locomotion performance of gaits over a range of lateral phase lag for quadruped, hexapod, myriapod, and sidewinder systems on different surfaces (Fig. 6). The quadrupedal experiments were performed on granular media (poppy seeds); other experiments were performed on hard ground. The duty factor for the hexapod, myriapod and the sidewinder systems were fixed to 0.5, and the duty factor for quadrupedal system was set to 0.75 for reference (see the Materials and Methods for additional experiment details). Note that in this section, there is no body undulation in all gaits.

We measured gait speed as body length traveled per gait cycle. Interestingly, the range of gaits showing theory-experiment discrepancy overlaps with the range of gaits that are not statically stable. Since our predictions are based on a 2D simulation, they cannot capture unstable behaviors, such as tipping over and falling to the ground. Therefore, we hypothesize that the theory-experiment discrepancy for the hexapods is caused by static instability. Note that our experiments on quadrupeds were performed on poppy seeds, where the ventral surface is in contact of the environment. In myriapod experiments, configurations tend to be mostly statically stable given their large number of legs. Therefore, the effect of static stability is only critical in hexapod experiments.

We next test our static instability hypothesis on the theory-experiment discrepancy. Unstable behaviors, such as tipping over and ground falling can be characterized by the roll and pitch of the robots. We recorded the body pitch and roll during the course of the robophysical hexapod gaits. The experimental data for these experiments over three gait settings ($D = 0.5$ $\Phi_{lat} = 0.15$, $D = 0.5$ $\Phi_{lat} = 0.45$, $D = 0.5$ $\Phi_{lat} = 0.65$) are compared in Fig. 7a. We observed that only the statically stable hexapod gait ($\Phi_{lat} = 0.45$) has both low pitch and low roll. The unstable hexapod gaits have either high roll angle ($\Phi_{lat} = 0.15$) or high pitch angle ($\Phi_{lat} = 0.65$). We calculated the average pitch and roll for each gait, and compared them with the numerical predictions of static stability. We observe that the range of low average pitch and roll overlaps with the range of statically stable gaits. When the hexapod body is in configurations with low roll and low pitch, the experimental data agree with the theoretical predictions.

Body-leg Coordination in Hildebrand Gait Formulation

Geometric Mechanics to Coordinate Lateral Body Undulation

As discussed in the previous sections, speed is not correlated with the the lateral phase lag. We observed from the relevant literature on lizards and myriapods Manton (1952); Farley and Ko (1997) that modulation of lateral phase lag is associated with changes in the lateral body undulation. Specifically, lizards increase the amplitude of their lateral body undulation during transitions from walking to trotting Farley and Ko (1997). Similarly, myriapods change their leg wave pattern (lateral phase lag) at high speed while simultaneously increasing lateral body undulation amplitude Manton (1952). Accordingly, we hypothesize that modulating the lateral phase lag can regulate the balance between speed and stability only if properly coordinated with lateral body undulation.

In this section, we introduce the lateral body bending angle α. (Fig. 2). We prescribed the lateral body undulation by propagating a wave of body bending propagating from head to tail Hirose and Yamada (2009):

$$\alpha(\phi_b, i) = A_\alpha \cos(\phi_b - 2\pi(i-1)\Phi^b_{lat}) \qquad (4)$$

where $\alpha(\phi_b, i)$ is the angle of i-th body joint at phase ϕ_c, $2\pi\Phi^b_{lat}$ is the phase lag between consecutive joints. For simplicity, we assume that spatial frequency of the lateral body undulation and the contact pattern is the same, i.e. $\Phi^b_{lat} = \Phi_{lat}$. In this way, we prescribed the lateral body undulation by its phase ϕ_b. The body shape can then be described as the phase of contact, ϕ_c, and the phase of lateral body undulation ϕ_b. These two independent phase variables represent a reduced shape space on a two-dimensional torus on which we can apply geometric mechanics gait design techniques to optimize body-limb coordination (Materials and Methods).

The geometric mechanics gait design framework separates the configuration space of a system into two spaces: the position space and the shape space. The position space represents the location (position and orientation) of a system relative to the world frame, while the shape space represents the internal shape (joint angles) of the system. The geometric mechanics framework then establishes a functional relationship to map velocities in the shape space into velocities in the position space; this functional relationship is often called a *local connection*. The curl of the local connection, which we call "height function" can then be used to design, analyze, and optimize gaits.

Using geometric mechanics tools Hatton and Choset (2015); Gong et al. (2018); Marsden and Ratiu (2013), we can derive a numerical height function to visually design gaits (Materials and Methods). Fig. 3 and Fig. 4 show examples of coordination between the lateral body undulation and contact phase with geometric mechanics. We also showed an example of coordinating the body undulation and contact pattern for sidewinding systems in Fig. S4. Once we designed a coordination pattern $\phi_c \to \phi_b$ in the reduced shape space, we obtained a prescription of contact pattern with coordinated body undulation.

We quantify the body-leg coordination by its phase lag: $\phi_{bc} : \phi_c - \phi_b$. Interestingly, we observe that the empirically calculated ϕ_{bc} has a linear relationship with Φ_{lat} (Fig. 8). We then seek to investigate its physical intuition. We first decompose the body-leg coordination to a single sub-unit (2 pairs of legs and one body joint). Hildebrand approach then allows us to prescribe the phase of each feet and the body bending. Previous work Chong et al. (2021) showed that it is desired that at the landing of HL/FR, the body is bent clockwise, and at the landing of HR/FL, the body is bent counterclockwise. With the empirical relation $\phi_{bc} \sim (\Phi_{lat} + 1/2)\pi$, the landing of FR and HL is symmetrically distributed around the peak of clockwise body bending; and the landing of FL and HR is symmetrically distributed around the peak of counterclockwise body bending. In this way, we posit that the empirical body-leg coordination is achieved by locally coordinating a sub-units of legged systems.

Numerical Prediction of Speed and Stability

Using the numerical simulation, we obtained a prediction of gait speed at a range of lateral phase lags and duty factors for the quadruped, hexapod, myriapod and sidewinder systems. The numerical prediction of the speed is shown in Fig. 5 (right panel). The static stability of gaits with body undulation is only slightly different from those with a straight

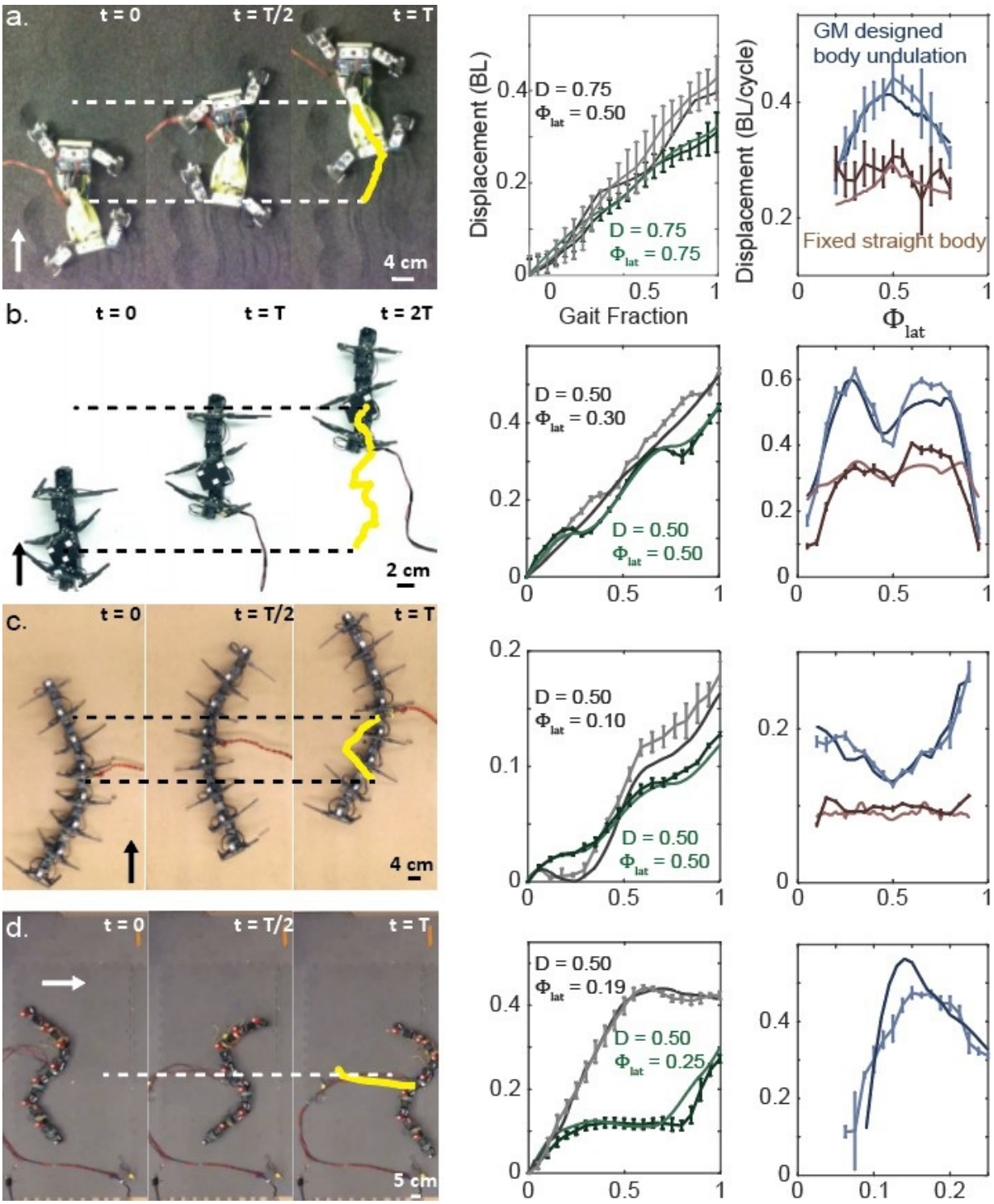

Figure 6. Verification of the theoretically generated gaits in the robotic models (left panel) Gait cycle of each robot (a: quadruped, D = 0.75 and Φ_{lat} = 0.5; b: hexapod, D = 0.5 and Φ_{lat}=0.3; c: myriapod, D = 0.5, Φ_{lat} = 0.1; d: sidewinder). The arrows show the direction of the locomotion and T is one gait cycle. The center of mass trajectories (yellow) are given in the last snapshots. (Middle panel) The comparison of simulations (plain curve) and experimental data (curve with error bar) on time evolution of displacement for each system. Two typical gaits (with geometric mechanics designed body undulation) are illustrated for each system. (Right panel) The relationship between the lateral phase lag, Φ_{lat}, and the displacement for system with fixed straight back (red) and system with coordinated lateral body undulation (blue). The color scheme and the plot frame in (b, c, d) is the same as in (a).

back (Fig. 5 left panel). The static stability for gaits with body undulation is depicted in Fig. S1.

We observed that modulating the lateral phase lag can regulate the balance between speed and stability if properly coordinated with lateral body undulation. The loss of static stability is compensated by a gain in speed only when the body and limb phases are properly coordinated.

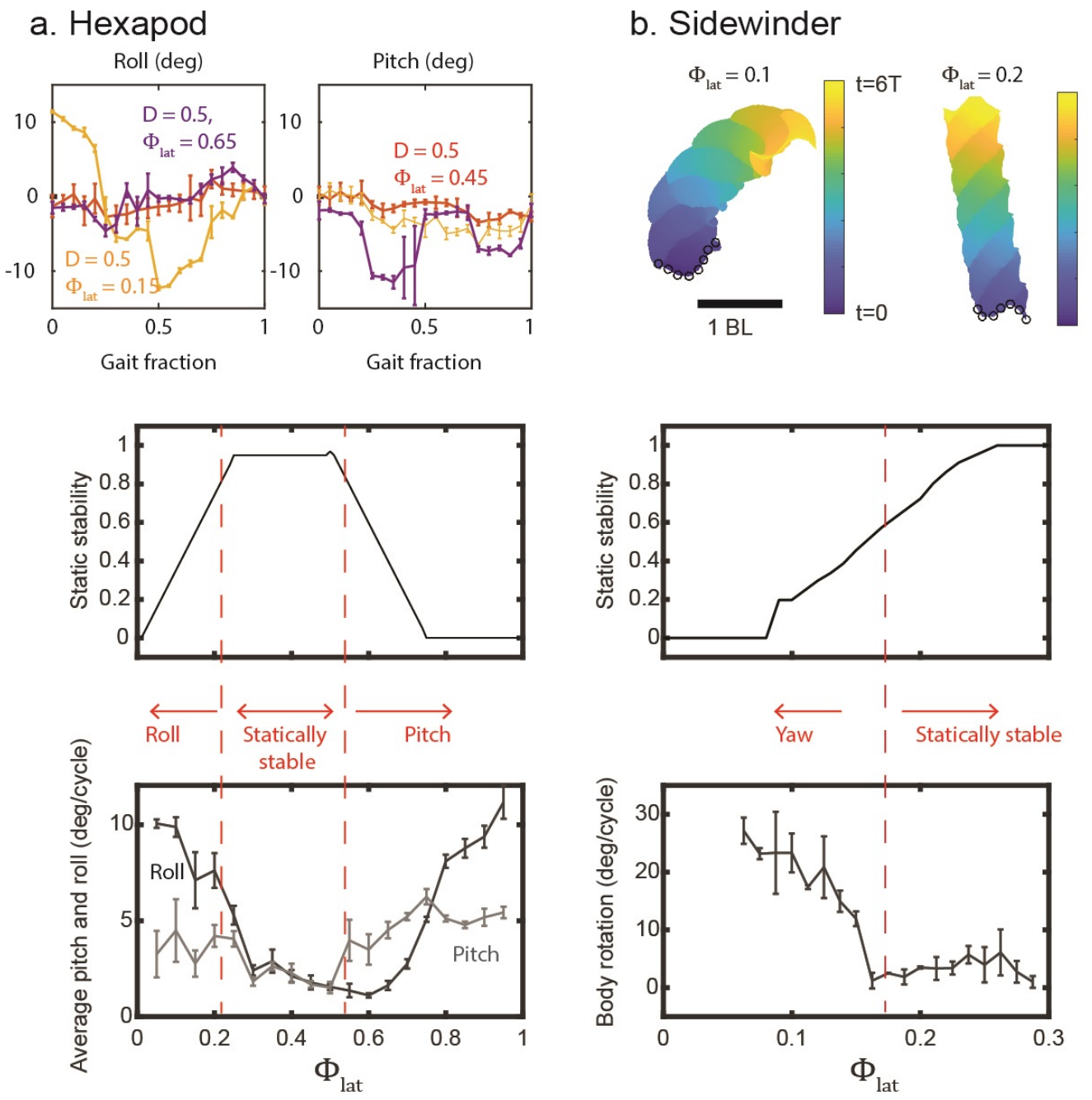

Figure 7. The effect of static stability on forward locomotion performance. (a. hexapod) In the top panel, the body roll and body pitch in experiments are recorded as a function of gait fraction. Three gaits ($D = 0.5$, $\Phi_{lat} = 0.65$ in purple; $D = 0.5$, $\Phi_{lat} = 0.45$ in red; and $D = 0.5$, $\Phi_{lat} = 0.15$ in yellow) in Hildebrand gait space are compared. In the middle row, we show the theoretical prediction of static stability as a function of lateral phase lag. In the bottom row, we show the average±SD experimental body roll and pitch as a function of the lateral phase lag. (b. sidewinders) We showed the trajectory of body motion in 6 gait cycles. The color represent gait periods. We marked the initial position of the robot in the black circles. In the middle panel, we showed the theoretical prediction of static stability as a function of the lateral phase lag. The turning angles are recorded as a function of lateral phase lag showed in the bottom panel of Fig 7b.

Experimental Results on Speed and Stability

We tested the locomotion performance of systems with discrete contact and coordinated lateral body undulation using robophysical models (Materials and Methods for details). We recorded the time evolution of displacement for two gaits in each system (Fig. 6). Our numerical predictions quantitatively agree with experiments not only in the average displacement per gait cycle, but also in the time evolution of the displacement.

The only notable theory-experiment discrepancies occur in the hexapod and the sidewinder systems. As discussed earlier, static instability can lead to theory-experiment discrepancy for hexapod due to the planar assumptions made in our theoretical model. Similarly, we speculate the theory-experiment discrepancy for sidewinders is a result of static instability.

We next studied the effect of static instability on sidewinders. We observed that some sidewinding gaits result

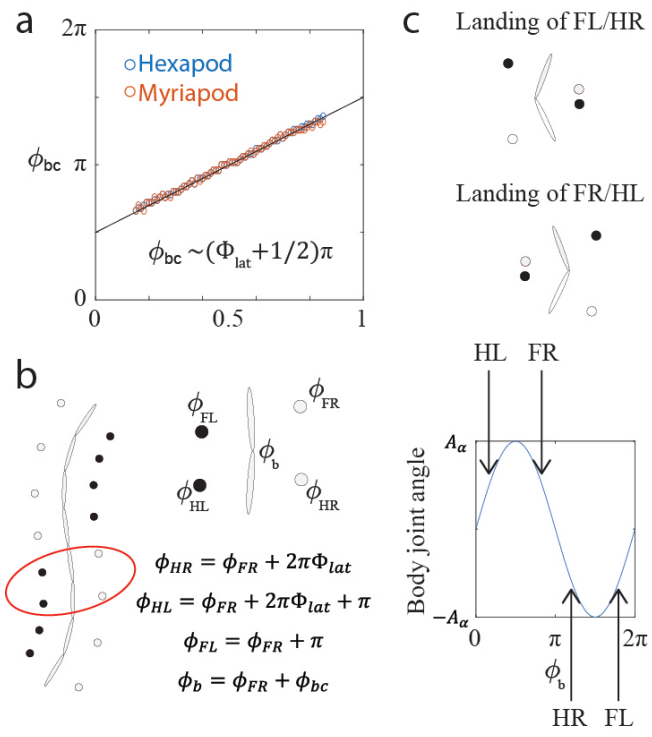

Figure 8. Physical Intuition of body-leg coordination (a) The relationship between Φ_{lat}, lateral phase lag, and ϕ_{bc}, the optimal phasing between body and leg. ϕ_{bc} is numerically calculated from height function (Fig. 3). The empirical data in hexapod (blue circle) and myriapod (red circle) are compared. (b) Consider a quadrupedal sub-unit (2 pairs of legs and one body-joint), the Hildebrand prescription allows us to write the phase relation of each leg and the body bending with respect to the fore right leg (FR). (c) It is desired that at the landing of FL (fore left) and HR (hind right) feet, the body is bent clockwise; and at the landing of FR and HL (hind left) feet, the body is bent counterclockwise Chong et al. (2021). Having the empirical relation $\phi_{bc} \sim (\Phi_{lat} + 1/2)\pi$, the landing of HL/FR and HR/FL are symmetrically distributed around the peaks of the bending, enabling body-bending coordination for each feet.

in significant yaw (Fig. 7b), such that the robot's path deviates from the desired straight-line course. We recorded the net yaw change per gait cycle for each gait and compared it with the numerical predictions of static stability. We observed that significant yaw only occurred at gaits with low static stability. As static stability increases (by increasing the lateral phase lag), the unmodelled turning vanished. This shows that theory-experiments discrepancy for the sidewinders are likely caused by static instability breaking the planar assumptions made in our theoretical model.

Discussion and Conclusion

Principles of gait modulation

In this paper, we have provided a general gait design framework that can guide control of a broad class of locomotors: multi-legged robots (with arbitrary pairs of legs) and a sidewinder robot. Specifically, we extended the Hildebrand gait formulation Hildebrand (1965, 1967), originally used to categorize symmetrical quadrupedal gaits, and combined it with the modern geometric mechanics tools to investigate its internal coordination. We showed that the symmetry properties in Hildebrand quadrupedal gaits are conserved for other locomotors: it is simple enough to enable physical interpretation of the gait parameters; on the other hand, it is sufficiently rich in content, offering a scheme to modulate gaits in a diversity of robot shapes and environments. In this way, our framework link the well-studied locomoting systems (such as quadrupeds and hexapods) to the less-studied systems (e.g., myriapods), offering opportunities to transfer among and compare different locomoting systems. For new robots with arbitrary pairs of legs or without leg, our framework can immediately provide effective gaits, which can then be further advanced by other methods such as adaptive control schemes and other data-based control algorithms.

Our gait principles reveal insights into proper contact scheduling for discrete contact systems during different modes of motion; these principles could then serve as a layer within in a robot's control architecture; or seeds to learning-based control algorithm. In our preliminary work Ozkan-Aydin et al. (2020*b*), we show that while direct application of our gait design tools cannot produce effective motions in rough terrains, some compliance (specifically: passive leg compliance) can greatly improve the gait performance on rough terrain and enable the gait control features discussed in this paper. Our proposed framework can not only simplify the gait design and modulation process for the robots of different morphology in various homogeneous environments, but also provides a guideline to the design controller for the robots that can navigate unstructured environments and overcome obstacles. In addition, our framework can also provide hypotheses and therefore give novel insights into the control principles behind biological systems.

Finally, our framework facilitate the hypothesis on the role of body undulation in multi-legged systems. These observations can act as guidelines in the control of a variety of legged robots. For example, in RHex Saranli et al. (2001), a hexapod with flexible legs attached to a rigid body, the duty factor is the only tuning parameter that can regulate the balance between speed and stability. In other cases, such as in Hoffman and Wood (2011), a segmented robot with a flexible backbone and contralateral legs coupled to a straight line (and therefore, have a fixed duty factor), the lateral phase lag acts as the salient parameter to balance between speed and stability when properly coordinated with lateral body undulation.

Insights from robotics to biological systems

In this paper, we showed that once two gait parameters (duty factor and lateral phase lag) are specified, the gait is readily prescribed and can then be analyzed with geometric tools. To explore gait tuning principles for locomoting systems, we quantitatively investigated the effect of modulating gait parameters on locomotion performance. As from Fig. 6, we observed that for robots with fixed straight body, the displacement per gait cycle is almost invariant of the changes of *lateral phase lag*, Φ_{lat}. On the other hand, only for those gaits where the body undulation is properly coordinated, the displacement can then be modulated by Φ_{lat}. This seemingly counter-intuitive observation can help us develop hypothesis on gait modulation principles.

In addition to these robotics applications, our proposed control principles can also offer explanatory power to some hypotheses about biological locomotion from a kinematic perspective. For example, biological myriapods (*Chilopoda*) can be categorized into direct-wave myriapods Manton (1952)) and retrograde-wave myriapods Manton (1952)). Direct-wave myriapods propagate their leg contact wave from tail to head (corresponding to $\Phi_{lat} < 0.5$ in our modified Hildebrand formulation) while retrograde-wave myriapods propagate their wave from head to tail ($\Phi_{lat} > 0.5$) Kuroda et al. (2014). Interestingly, Manton Manton (1952) showed that there is no significant lateral body undulation in direct-wave myriapods regardless of their speed; instead, the only significant gait modulation at high speed is a decrease in duty factor. On the other hand, gait modulation in retrograde-wave myriapods is much more complicated: they not only decrease the duty factor, but also increase the lateral phase lag. More importantly, they exhibit characteristic lateral body undulation at high speeds Manton (1952); Anderson et al. (1995). This observation is consistent with our proposed control principle that tuning the lateral phase lag is effective to improve speed only if accompanied with properly coordinated lateral body undulation. Moreover, the contribution from lateral body undulation is greater for retrograde-wave myriapod locomotion than for direct-wave myriapods. This may be one reason why lateral body undulation is only characteristic of retrograde-wave myriapod.

Materials and Methods

Geometric Mechanics

We used tools from geometric mechanics, the application of differential geometry concepts to rigid body mechanics, to design the coordination between body undulation and contact patterns. In this section, we provide a concise overview of the tools used to design the coordination patterns. For a more detailed and comprehensive review, we refer readers to Gong et al. (2018); Marsden and Ratiu (2013); Chong et al. (2021).

The geometric mechanics gait design framework separates the configuration space of a system into two spaces: the position space and the shape space. The position space represents the location (position and orientation) of a system relative to the world frame, while the shape space represents the internal shape (joint angles) of the system. The geometric mechanics framework then establishes a functional relationship to map velocities in the shape space into velocities in the position space; this functional relationship is often called a *local connection*.

Reduced Equation of Motion In kinematic systems where the frictional forces dominate the inertial forces, the equations of motion can be approximated by:

$$\boldsymbol{\xi} = \boldsymbol{A}(\boldsymbol{\Phi})\dot{\boldsymbol{\Phi}}, \tag{5}$$

where $\boldsymbol{\xi} = [\xi_x \ \xi_y \ \xi_\theta]^T \in g$ denotes the body velocity in the forward (x), lateral (y), and yaw (θ) directions; $\boldsymbol{\Phi}$ denotes the internal shape variables (in our case, $\boldsymbol{\Phi} = [\phi_c \ \phi_b]^T$, representing the contact phase and the lateral body undulation phase); $\boldsymbol{A}(\boldsymbol{\Phi})$ is the local connection matrix, which encodes environmental substrate interactions.

Numerical Derivation of the Local Connection Matrix As shown in Hatton et al. (2013), the local connection matrix $\boldsymbol{A}$ can be numerically derived via force and torque balances. The equations for the force and torque balance require a model of the ground reaction forces (GRF), such as granular material interaction and ground friction. We summarize the GRF formula for our four robots above. Further details on the local connection derivation can be found in the Supplementary Material.

Connection Vector Fields and Height Functions Once we obtain the local connection matrix, we can further analyze the system kinematics during locomotion. Each row of the local connection matrix $\boldsymbol{A}$ corresponds to a component direction of the body velocity. Each row of the local connection matrix over the shape space then formed a connection vector field. In this way, the body velocities in the forward, lateral, and rotational directions are respectively computed as the dot product of connection vector fields and the shape velocity $\dot{\boldsymbol{\Phi}}$.

A periodic gait can be represented as a closed curve in the shape space. The displacement resulting from a gait, $\partial\chi$, can be approximated by:

$$\begin{pmatrix}\Delta x\\ \Delta y\\ \Delta\theta\end{pmatrix} = \int_{\partial\chi} \boldsymbol{A}(\boldsymbol{\Phi})d\boldsymbol{\Phi}. \tag{6}$$

According to Stokes' Theorem, the line integral along a closed curve $\partial\chi$ is equal to the surface integral of the curl of $\boldsymbol{A}(\boldsymbol{\Phi})$ over the surface enclosed by $\partial\chi$:

$$\int_{\partial\chi} \boldsymbol{A}(\boldsymbol{\Phi})d\boldsymbol{\Phi} = \iint_{\chi} \boldsymbol{\nabla}\times\boldsymbol{A}(\boldsymbol{\Phi})d\phi_c d\phi_b, \tag{7}$$

where χ denotes the surface enclosed by $\partial\chi$. The curl of the connection vector field, $\boldsymbol{\nabla}\times\boldsymbol{A}(\boldsymbol{\Phi})$, is referred to as the *height function*. The three rows of the vector field $\boldsymbol{A}(\boldsymbol{\Phi})$ can thus produce three height functions in the forward, lateral and rotational direction, respectively.

The height function derivation simplifies the gait design problem to drawing a closed path in a Euclidean shape space. The body displacement from a path can be approximated by the integral of the surface enclosed by that path.

Toroidal Shape Spaces In our gait prescription, the two shape variables are parameterized as cyclic phases, resulting in a toroidal shape space (T^2) Kobayashi and Nomizu (1963). Examples of height functions on toroidal shape spaces are shown in Fig. 3b. The shape variables $\boldsymbol{\Phi} = [\phi_c, \ \phi_b]^T \in T^2$ correspond to the phase of contact and the phase of the lateral body undulation, respectively. A gait path (solid purple curve Fig. 3b) is a closed curve in the toroidal shape space, but as it is a non-Euclidean space, there is no clear "surface" enclosed by the path.

To form an enclosed surface, Gong et al., Gong et al. (2018) introduced the notion of two assistive lines in the Euclidean parameterization of the toroidal shape space. This allows a surface integral to be calculated (Fig. 3b, the area within solid lines is subtracted from the area of the surface enclosed in the upper left corner). For simplicity, in our optimization we assumed that the mapping between the two phase variables is linear and have the same temporal frequency, i.e., $\phi_b = \partial\chi(\phi_c) = \phi_c + \phi_0$, where ϕ_0 is the

Robot	*GRF Formula*	*Reference*
Quadruped	Poppy Seed RFT	McInroe et al. (2016); Chong et al. (2021)
Hexapod	Anisotropic Coulomb Friction	Walker and Leine (2019); Transeth et al. (2008)
Myriapod	Anisotropic Coulomb Friction	Walker and Leine (2019); Transeth et al. (2008)
Sidewinder	Isotropic Coulomb Friction	Chong et al. (2020); Rieser et al. (2019)

Table 1. The ground reaction force formula that we used to model quadrupeds, hexapods, myriapods, and sidewinders robophysical systems.

phase offset between lateral body undulation and contact pattern to be optimized.

Simulation

We performed a numerical simulation to predict locomotive performance, and compared these results to those obtained from robophysical experiments. Specifically, we prescribed the contact state and the joint angle of each leg by a single variable, ϕ_c, using Eq. 2 and Eq. 3. Similarly, we prescribed the lateral body undulation by another variable, ϕ_b, using Eq. 4. The amplitudes of leg and body joint angles are listed below.

Robot	A_θ	A_α
Quadruped	30°	30°
Hexapod	10°	10°
Myriapod	12°	17°
Sidewinder	N/A	$5.6L$ (rad)

Note that the amplitude of sidewinder body undulation is related to the lateral phase lag, such that the "relative curvature," that is, the maximum curvature of the backbone of limbless locomotors Astley, Mendelson, Dai, Gong, Chong, Rieser, Schiebel, Sharpe, Hatton, Choset et al. (2020); Sharpe et al. (2015); Rieser et al. (2019), remains constant.

In the previous section, we described the method by which we find the body-limb coordination function $\partial\chi : \phi_c \to \phi_b$. Therefore, the shape variable $\mathbf{\Phi}$ and shape velocity $\dot{\mathbf{\Phi}}$ can be rewritten as:

$$\mathbf{\Phi} = \begin{bmatrix} \phi_c \\ \partial\chi(\phi_c) \end{bmatrix}, \quad \dot{\mathbf{\Phi}} = \begin{bmatrix} 1 \\ \frac{\boldsymbol{d}\partial\chi(\phi_c)}{\boldsymbol{d}\phi_c} \end{bmatrix} \dot{\phi}_c \tag{8}$$

Then we integrate the locomotion with the standard ordinary differential equation Hatton and Choset (2015):

$$g(t) = \int_0^t T_e L_{g(\phi_c)} A(\mathbf{\Phi}) \boldsymbol{d}\mathbf{\Phi} \tag{9}$$

$$= \int_0^t T_e L_{g(\phi_c)} A(\begin{bmatrix} \phi_c \\ \partial\chi(\phi_c) \end{bmatrix}) \begin{bmatrix} 1 \\ \frac{\boldsymbol{d}\partial\chi(\phi_c)}{\boldsymbol{d}\phi_c} \end{bmatrix} \boldsymbol{d}\phi_c, \tag{10}$$

where $g = (x, y, \alpha) \in SE(2)$ represents the body frame position and rotation Murray (2017). Note that $T_e L_g$ is the left lifted action with respect to the coordinates of g:

$$T_e L_g = \begin{bmatrix} \cos(\alpha) & -\sin(\alpha) & 0 \\ \sin(\alpha) & \cos(\alpha) & 0 \\ 0 & 0 & 1 \end{bmatrix} \tag{11}$$

Integrate the ordinary differential equation throughout one period (from $t = 0$ to $t = 2\pi$), we obtain the trajectory of locomotor and can determine the predicted displacements in the forward, lateral, and rotational directions over one gait cycle. Note that we neglect the inertia effect in the simulation.

Robophysical Experiments

Robotic Models All of the robophysical models were designed in Solidworks and printed using Stratasys Dimension Elite 3D Printer. They are powered with an external power supply (12 V, 5A) and controlled by DYNAMIXEL SDK (using Matlab programming language) which interfaces with the servo motors via Robotis USB2Dynamixel controller. All the robots have open-loop control such that gait parameters are not changed during time and the control signals (servo positions) continue to be sent as a function of time, regardless of external forces or the tracking accuracy of the servos.

Quadruped robot (Fig.S4a, 450 g., ∼40 cm long, Ozkan Aydin et al. (2017)) has four 2 DoF legs and an actuated trunk. Each limb has two Dynamixel XL-320 servos (stall torque= 0.39 [N.m]) to control the vertical position and the step size of the leg (h= 45mm, Fig.S4a). The body joint servo (Dynamixel AX-12) controls the horizontal bending. The legs have cube shape with 24X24 mm^2 surface area.

Hexapod robot (Fig.S4b, 300 g., ∼25 cm long) has a segmented body (3 segments) with pairs of legs in each segment. The vertical and horizontal motion of the legs in a segment are coupled (out-of-phase) and controlled by two Dynamixel XL-320 servos (Fig.S4b). The body joint servos (Dynamixel XL-320) controls the horizontal bending of the segments. The legs have a pointy toe.

Myriapod robot (Fig.S4c, ∼1000 g., ∼72 cm long) has a segmented body (8 segments) similar to the hexapod robot Ozkan-Aydin et al. (2020*a*). Each segment has a pairs of rigidly connected legs (l= 12 cm). There are three servos (Dynamixel XL-320) in each segment; one controls horizontal body bending and two control the fore/aft and up/down motion of the legs (Fig.S4b).

Sidewinder robot has seven segments in which there are two joints connected at an angle of 90^o (Fig.S4c). The joint angles (horizontal and vertical motion of each segment) are controlled by AX-12 servo motors (stall torque = 1.5 [N.m]). The horizontal motors vary lateral wave and the vertical motors create a changing contact pattern.

Experimental Setups and Data Analysis In all experiments, we used Optitrack motion capture system (including 4-6 Naturalpoint, Flex13 cameras, 120 fps and Motive software) to capture the position and the orientation of the reflective markers attached to the robots. The data was analyzed in Matlab.

Quadruped robot experiments were performed on a trackway filled with ∼1 mm diameter poppy seeds Ozkan Aydin et al. (2017). Before each experiment we fluidized the bed using four vacuums to prepare a uniform loosely packed state. Every experiments (with different gait parameters) were repeated 3 times (total 9 cycles).

Hexapod and myriapod robot experiments were performed on a cardboard and particle board, respectively. Before each experiment, the joint angles were set to their neutral position. The robots were allowed to run for three cycles (5 trials/gait).

Sidewinder experiments were performed on an arena covered with foam mats to reduce slip. Each experiments were started from the same position and repeated 3 times (5-6 cycles per each trials).

References

Anderson, B., Shultz, J. and Jayne, B. (1995), 'Axial kinematics and muscle activity during terrestrial locomotion of the centipede scolopendra heros', *Journal of Experimental Biology* **198**(5), 1185–1195.

Aoi, S., Tanaka, T., Fujiki, S., Funato, T., Senda, K. and Tsuchiya, K. (2016), 'Advantage of straight walk instability in turning maneuver of multilegged locomotion: a robotics approach', *Scientific reports* **6**, 30199.

Astley, H. C., Gong, C., Dai, J., Travers, M., Serrano, M. M., Vela, P. A., Choset, H., Mendelson, J. R., Hu, D. L. and Goldman, D. I. (2015), 'Modulation of orthogonal body waves enables high maneuverability in sidewinding locomotion', *Proceedings of the National Academy of Sciences* **112**(19), 6200–6205.

Astley, H. C., Mendelson, J. R., Dai, J., Gong, C., Chong, B., Rieser, J. M., Schiebel, P. E., Sharpe, S. S., Hatton, R. L., Choset, H. et al. (2020), 'Surprising simplicities and syntheses in limbless self-propulsion in sand', *Journal of Experimental Biology* **223**(5).

Astley, H. C., Rieser, J. M., Kaba, A., Paez, V. M., Tomkinson, I., Mendelson, J. R. and Goldman, D. I. (2020*a*), 'Side-impact collision: mechanics of obstacle negotiation in sidewinding snakes', *Bioinspiration & Biomimetics* **15**(6), 065005.

Astley, H. C., Rieser, J. M., Kaba, A., Paez, V. M., Tomkinson, I., Mendelson, J. R. and Goldman, D. I. (2020*b*), 'Side-impact collision: mechanics of obstacle negotiation in sidewinding snakes', *Bioinspiration & Biomimetics* **15**(6), 065005.

Bai, S., Low, K. H., Seet, G. and Zielinska, T. (1999), A new free gait generation for quadrupeds based on primary/secondary gait, *in* 'Proceedings 1999 IEEE International Conference on Robotics and Automation (Cat. No. 99CH36288C)', Vol. 2, IEEE, pp. 1371–1376.

Bellicoso, C. D., Jenelten, F., Gehring, C. and Hutter, M. (2018), 'Dynamic locomotion through online nonlinear motion optimization for quadrupedal robots', *IEEE Robotics and Automation Letters* **3**(3), 2261–2268.

Byl, K. (2008), Metastable legged-robot locomotion, PhD thesis, Massachusetts Institute of Technology.

Chong, B., Aydin, Y. O., Gong, C., Sartoretti, G., Wu, Y., Rieser, J. M., Xing, H., Schiebel, P. E., Rankin, J. W., Michel, K. B. et al. (2021), 'Coordination of lateral body bending and leg movements for sprawled posture quadrupedal locomotion', *The International Journal of Robotics Research* **40**(4-5), 747–763.

Chong, B., Wang, T., Rieser, J. M., Kaba, A., Choset, H. and Goldman, D. I. (2020), Frequency modulation of body waves to improve performance of limbless robots, *in* 'Robotics: Science and Systems'.

Crespi, A., Lachat, D., Pasquier, A. and Ijspeert, A. J. (2008), 'Controlling swimming and crawling in a fish robot using a central pattern generator', *Autonomous Robots* **25**(1), 3–13.

Dutta, S., Parihar, A., Khanna, A., Gomez, J., Chakraborty, W., Jerry, M., Grisafe, B., Raychowdhury, A. and Datta, S. (2019), 'Programmable coupled oscillators for synchronized locomotion', *Nature communications* **10**(1), 1–10.

Farley, C. T. and Ko, T. C. (1997), 'Mechanics of locomotion in lizards.', *Journal of Experimental Biology* **200**(16), 2177–2188.

Frolich, L. M. and Biewener, A. A. (1992), 'Kinematic and electromyographic analysis of the functional role of the

body axis during terrestrial and aquatic locomotion in the salamander ambystoma tigrinum', *Journal of Experimental Biology* **162**(1), 107–130.

Gong, C., Whitman, J., Grover, J., Chong, B., Ren, R. and Choset, H. (2018), Geometric motion planning for systems with toroidal and cylindrical shape spaces, *in* 'Dynamic Systems and Control Conference'.

Hatton, R. L. and Choset, H. (2015), 'Nonconservativity and noncommutativity in locomotion', *The European Physical Journal Special Topics* **224**(17-18), 3141–3174.

Hatton, R. L., Ding, Y., Choset, H. and Goldman, D. I. (2013), 'Geometric visualization of self-propulsion in a complex medium', *Physical review letters* **110**(7), 078101.

Hildebrand, M. (1965), 'Symmetrical gaits of horses', *Science* **150**(3697), 701–708.

Hildebrand, M. (1967), 'Symmetrical gaits of primates', *American Journal of Physical Anthropology* **26**(2), 119–130.

Hildebrand, M. (1980), 'The adaptive significance of tetrapod gait selection', *American Zoologist* **20**(1), 255–267.

Hirose, S. and Yamada, H. (2009), 'Snake-like robots [tutorial]', *IEEE Robotics & Automation Magazine* **16**(1), 88–98.

Hoffman, K. L. and Wood, R. J. (2011), 'Myriapod-like ambulation of a segmented microrobot', *Autonomous Robots* **31**(1), 103.

Hoyt, D. F. and Taylor, C. R. (1981), 'Gait and the energetics of locomotion in horses', *Nature* **292**(5820), 239–240.

Hwangbo, J., Lee, J., Dosovitskiy, A., Bellicoso, D., Tsounis, V., Koltun, V. and Hutter, M. (2019), 'Learning agile and dynamic motor skills for legged robots', *Science Robotics* **4**(26), eaau5872.

Ijspeert, A. J., Crespi, A., Ryczko, D. and Cabelguen, J.-M. (2007), 'From swimming to walking with a salamander robot driven by a spinal cord model', *science* **315**(5817), 1416–1420.

Kafkafi, N. and Golani, I. (1998), 'A traveling wave of lateral movement coordinates both turning and forward walking in the ferret', *Biological cybernetics* **78**(6), 441–453.

Kalakrishnan, M., Buchli, J., Pastor, P., Mistry, M. and Schaal, S. (2010), Fast, robust quadruped locomotion over challenging terrain, *in* '2010 IEEE International Conference on Robotics and Automation', IEEE, pp. 2665–2670.

Kelly, S. D. and Murray, R. M. (1995), 'Geometric phases and robotic locomotion', *Journal of Robotic Systems* **12**(6), 417–431.

Kobayashi, S. and Nomizu, K. (1963), *Foundations of differential geometry*, Vol. 1, Interscience publishers New York.

Kuroda, S., Kunita, I., Tanaka, Y., Ishiguro, A., Kobayashi, R. and Nakagaki, T. (2014), 'Common mechanics of mode switching in locomotion of limbless and legged animals', *Journal of the Royal Society interface* **11**(95), 20140205.

Manton, S. (1952), 'The evolution of arthropodan locomotory mechanisms—part 3. the locomotion of the chilopoda and pauropoda.', *Zoological Journal of the Linnean Society* **42**(284), 118–167.

Marsden, J. E. and Ratiu, T. S. (2013), *Introduction to mechanics and symmetry: a basic exposition of classical mechanical systems*, Vol. 17, Springer Science & Business Media.

Marvi, H., Gong, C., Gravish, N., Astley, H., Travers, M., Hatton, R. L., Mendelson, J. R., Choset, H., Hu, D. L. and Goldman, D. I. (2014), 'Sidewinding with minimal slip: Snake and robot ascent of sandy slopes', *Science* **346**(6206), 224–229.

Mazouchova, N., Umbanhowar, P. B. and Goldman, D. I. (2013), 'Flipper-driven terrestrial locomotion of a sea turtle-inspired robot', *Bioinspiration & biomimetics* **8**(2), 026007.

McGhee, R. B. and Frank, A. A. (1968), 'On the stability properties of quadruped creeping gaits', *Mathematical Biosciences* **3**, 331–351.

McInroe, B., Astley, H. C., Gong, C., Kawano, S. M., Schiebel, P. E., Rieser, J. M., Choset, H., Blob, R. W. and Goldman, D. I. (2016), 'Tail use improves performance on soft substrates in models of early vertebrate land locomotors', *Science* **353**(6295), 154–158.

McKenna, J. C., Anhalt, D. J., Bronson, F. M., Brown, H. B., Schwerin, M., Shammas, E. and Choset, H. (2008), Toroidal skin drive for snake robot locomotion, *in* '2008 IEEE International Conference on Robotics and Automation', IEEE, pp. 1150–1155.

Murray, R. M. (2017), *A mathematical introduction to robotic manipulation*, CRC press.

Ostrowski, J. and Burdick, J. (1998), 'The geometric mechanics of undulatory robotic locomotion', *The international journal of robotics research* **17**(7), 683–701.

Owaki, D., Kano, T., Nagasawa, K., Tero, A. and Ishiguro, A. (2013), 'Simple robot suggests physical interlimb communication is essential for quadruped walking', *Journal of The Royal Society Interface* **10**(78), 20120669.

Ozkan-Aydin, Y., Chong, B., Aydin, E. and Goldman, D. I. (2020*a*), A systematic approach to creating terrain-capable hybrid soft/hard myriapod robots, *in* '2020 3rd IEEE International Conference on Soft Robotics (RoboSoft)', pp. 156–163.

Ozkan-Aydin, Y., Chong, B., Aydin, E. and Goldman, D. I. (2020*b*), A systematic approach to creating terrain-capable hybrid soft/hard myriapod robots, *in* '2020 3rd IEEE International Conference on Soft Robotics (RoboSoft)', IEEE, pp. 156–163.

Ozkan Aydin, Y., Chong, B., Gong, C., Rieser, J. M., Rankin, J. W., Michel, K., Nicieza, A. G., Hutchinson, J., Choset, H. and Goldman, D. I. (2017), Geometric mechanics applied to tetrapod locomotion on granular media, *in* M. Mangan, M. Cutkosky, A. Mura, P. F. Verschure, T. Prescott and N. Lepora, eds, 'Biomimetic and Biohybrid Systems', Springer International Publishing, Cham, pp. 595–603.

Park, H.-W., Wensing, P. M. and Kim, S. (2017), 'High-speed bounding with the mit cheetah 2: Control design and experiments', *The International Journal of Robotics Research* **36**(2), 167–192.

Popovic, M. B., Goswami, A. and Herr, H. (2005), 'Ground reference points in legged locomotion: Definitions, biological trajectories and control implications', *The international journal of robotics research* **24**(12), 1013–1032.

Rieser, J. M., Gong, C., Astley, H. C., Schiebel, P. E., Hatton, R. L., Choset, H. and Goldman, D. I. (2019), 'Geometric phase and dimensionality reduction in locomoting living systems', *arXiv preprint arXiv:1906.11374* .

Saranli, U., Buehler, M. and Koditschek, D. E. (2001), 'Rhex: A simple and highly mobile hexapod robot', *The International Journal of Robotics Research* **20**(7), 616–631.

Sartoretti, G., Paivine, W., Shi, Y., Wu, Y. and Choset, H. (2019), 'Distributed learning of decentralized control policies for articulated mobile robots', *IEEE Transactions on Robotics* **35**(5), 1109–1122.

Shammas, E. A., Choset, H. and Rizzi, A. A. (2007), 'Geometric motion planning analysis for two classes of underactuated mechanical systems', *The International Journal of Robotics Research* **26**(10), 1043–1073.

Shapere, A. and Wilczek, F. (1989), *Geometric phases in physics*, World Scientific.

Sharpe, S. S., Koehler, S. A., Kuckuk, R. M., Serrano, M., Vela, P. A., Mendelson, J. and Goldman, D. I. (2015), 'Locomotor benefits of being a slender and slick sand swimmer', *Journal of Experimental Biology* **218**(3), 440–450.

Sun, H. C. and Metaxas, D. N. (2001), Automating gait generation, *in* 'Proceedings of the 28th annual conference on Computer graphics and interactive techniques', pp. 261–270.

Tan, J., Zhang, T., Coumans, E., Iscen, A., Bai, Y., Hafner, D., Bohez, S. and Vanhoucke, V. (2018), 'Sim-to-real: Learning agile locomotion for quadruped robots', *arXiv preprint arXiv:1804.10332* .

Tesch, M., Lipkin, K., Brown, I., Hatton, R., Peck, A., Rembisz, J. and Choset, H. (2009), 'Parameterized and scripted gaits for modular snake robots', *Advanced Robotics* **23**(9), 1131–1158.

Transeth, A. A., Leine, R. I., Glocker, C. and Pettersen, K. Y. (2008), '3-d snake robot motion: nonsmooth modeling, simulations, and experiments', *IEEE transactions on robotics* **24**(2), 361–376.

Walker, S. and Leine, R. (2019), 'Set-valued anisotropic dry friction laws: formulation, experimental verification and instability phenomenon', *Nonlinear Dynamics* **96**(2), 885–920.

Wettergreen, D. and Thorpe, C. (1992), Gait generation for legged robots, *in* 'IEEE International Conference on Intelligent Robots and Systems'.

Wright, C., Johnson, A., Peck, A., McCord, Z., Naaktgeboren, A., Gianfortoni, P., Gonzalez-Rivero, M., Hatton, R. and Choset, H. (2007), Design of a modular snake robot, *in* '2007 IEEE/RSJ International Conference on Intelligent Robots and Systems', IEEE, pp. 2609–2614.